Effect of Cholesterol on Viscoelastic Properties of Dipalmitoylphosphatidylcholine Multibilayers As Measured by a Laser-Induced Ultrasonic Probe[†]

M. Y. El-Sayed, T. A. Guion, and M. D. Fayer*

Department of Chemistry, Stanford University, Stanford, California 94305

Received December 9, 1985; Revised Manuscript Received February 27, 1986

ABSTRACT: Using a novel laser-induced ultrasonic probe, we have examined the bulk viscoelastic properties of fully hydrated dipalmitoylphosphatidylcholine (DPPC) aligned multibilayers in terms of the anisotropic in-plane elastic stiffness (C_{11}) and viscosity (η_{11}). Our measurements of C_{11} are in accord with those reported on Brillouin light scattering on a similar system. Our measurements on viscosity are the first of their kind and are, on the average, a factor of 10 lower than microviscosities estimated by spectroscopic techniques. We report the first comprehensive study of the effects of cholesterol on the bulk mechanical properties of DPPC multibilayers. At temperatures above the phase transition temperature of DPPC (T_c), an increase in both C_{11} and η_{11} is noticed when cholesterol is incorporated in the multibilayers. However, at temperatures below T_c, no measurable changes are detected in either C_{11} or η_{11}. These results, reflecting changes in the bulk viscoelastic properties of the multibilayers, differ from the changes reported by local fluidity parameters in that the latter indicate a decrease in the bilayer fluidity in the presence of cholesterol above T_c and an *increase* below T_c ("dual effect" of cholesterol). Our data suggest that the "dual effect" of cholesterol is noticeable only on a molecular scale. Increasing cholesterol concentrations higher than 20 mol % cease to further affect C_{11} or η_{11} of the DPPC multibilayers. This agrees with various results reported in the literature, by techniques measuring the local effects of cholesterol, and supports the changes in molecular organization postulated to occur when cholesterol concentration reaches 20 mol % in the lipid bilayers.

Cholesterol is an important and abundant constituent of most eukaryotic membranes. In cell membranes, cholesterol constitutes up to 50 mol % of the lipid. The physiological significance of cholesterol and its effect on membrane fluidity has been the subject of many recent articles and reviews (Shinitzky et al., 1983a,b). The interactions of cholesterol with phospholipid molecules (the other major lipid component of cell membranes) have been actively examined through model systems (bilayers, vesicles, and micelles) for the past decade (Jain, 1975; Phillips, 1972; Demel & De Kruijff, 1976). Various techniques including electron spin resonance (ESR) spectroscopy (Recktenwald & McConnell, 1981; Shimshick & McConell, 1973, NMR spectroscopy (Cullis, 1976; Tilcock et al., 1982), electron microscopy (Copeland, & McConnell, 1980; Lentz et al., 1980), IR spectroscopy (Cortijo & Chapman, 1981), fluorescence spectroscopy (Vanderkooi, 1974; Shinitzky & Barenholz, 1978), and differential scanning ca-lorimetry (DSC) (Papahadjopoulos et al., 1973; Mabrey et al., 1978; Estep et al., 1978) have been used to study the effect that cholesterol has on the mechanical properties and fluidity of the cholesterol/phospholipid model system. All these techniques have different definitions of the membrane fluidity. The term "membrane fluidity" has been used in the literature to describe two different types of motion: (1) the vibrational or rotational movement of a group on a molecule, often measured by NMR and ESR; (2) the diffusivity or transla-tional motion of a molecule. Although both classes of prop-erties depend on the "free space" available in a two-dimensional lattice (Blank, 1962; Blank & Britten, 1965), when different samples are compared, the trends can be easily masked by a large variety of competing processes (Schreier et al., 1978). Furthermore, all these techniques measure changes in the molecular environment of the bilayer rather than bulk changes in the bilayer plane.

More recently, viscosity and lateral compressibility mea-surements have been performed on multibilayers according to the theories of wave propagation through lipid multibilayers

(Crilly & Earnshaw, 1983; Sakanishi et al., 1979; Mitaku et al., 1978; LePesant et al., 1978). The advantages of this approach to study lipid bilayers are numerous: (1) it is a nonobtrusive technique that does not require the use of a molecular probe that may alter the properties of the bilayer, (2) it provides a *direct* measure to the physical parameters in question and requires no molecular model to interpret the results, and (3) it results in quantitative numbers for the bulk viscoelastic parameters of the bilayer system, an analysis that until now has not been possible.

This laboratory has previously used laser induced phonon spectroscopy (LIPS) to monitor the dynamic properties of dilinoleoylphosphatidylcholine (DLPC) aligned bilayers (Eyring & Fayer, 1985). In this technique sample excitation by two crossed 100-ps laser pulses generates a longitudinal ultrasonic wave whose wavelength depends on the crossing angle. In these experiments, the acoustic wave propagates parallel to the bilayer planes. The ultrasonic velocity and attenuation are monitored through the diffraction of a variably delayed probe pulse. The velocity measures the lateral area compressibility of the bilayers, while the attenuation is related to the viscosity.

This method of acoustic wave generation is more flexible than the previously used Billouin scattering technique (Le-Pesant et al., 1978), in that it can generate waves of lower frequency ($<10^8$ Hz vs. $>10^9$ Hz) and can accurately measure large attenuations. This work uses the LIPS experiment to study the effects of cholesterol on the bulk viscosity and elastic stiffness of aligned dipalmitoylphosphatidylcholine (DPPC) multibilayers in the liquid-crystalline and gel states.

EXPERIMENTAL PROCEDURES

Materials and Samples

Dipalmitoylphosphatidylcholine (Sigma) was used without further purification. Cholsterol (Calbiochem) was dissolved in chloroform and filtered through a pore size of 0.1 μm to remove dust particles. The $CHCl_3$ was blown off and the dried stock stored desiccated in a freezer. HEPES [N-(2-hydroxyethyl)piperazine-N'-2-ethanesulfonic acid] (Sigma) was made to 50 mM, pH 7.5, and also filtered to remove dust particles. Deionized water was used throughout this work.

Sample Preparation. The appropriate amounts of cholesterol and DPPC were placed in a small glass vial and codissolved in $CHCl_3$. The $CHCl_3$ was then blown off with nitrogen gas and the sample lyophilized to remove any remaining traces of $CHCl_3$. The resulting mixture was then hydrated to $\sim$8 wt % and allowed to equilibrate at least 24 h. Approximately 10–15 mg of the lipid–cholesterol paste was sandwiched between two silica optical flats, separated by a 280-μm Teflon spacer (except in the case of the pure DPPC samples, where a 125-μm Teflon spacer was used). This assembly was inserted into a variable-temperature cell that could be heated resistively up to 200 °C. The temperature was maintained by a temperature controller and monitored with a 3-mm platinum resistance thermometer (GSO 330; Omega Engineering, Inc., Stamford, CT) that was inserted into a hole drilled into one of the optical flats parallel to the face (the bottom one of the sandwich setup). The temperature was controlled to within $\pm$0.2 °C.

Alignment of the sample into planar, multibilayer arrays was achieved by a modified form of the Asher and Pershan method (Powers & Clark, 1975; Asher & Pershan, 1979). The sample was heated to $\sim$80 °C (well above the gel–liquid-crystalline phase transition temperature) and gently sheared laterally by modulating the applied pressure on the sides of
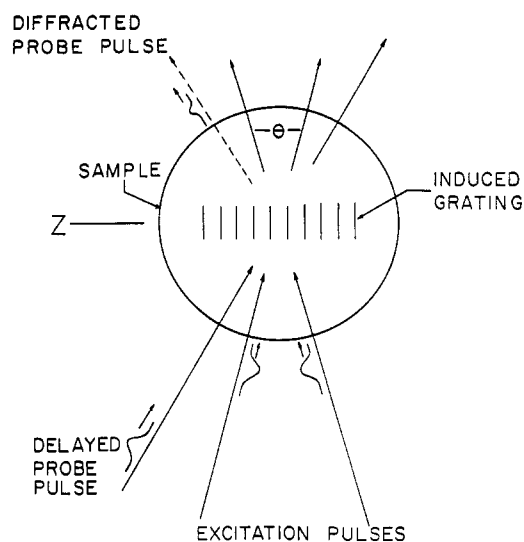

FIGURE 1: Schematic illustration of the LIPS experiment. The crossed excitation pulses generate a standing longitudinal acoustic wave in the aligned lipid multibilayers having the wavelength and orientation (wave vector along z) of the optical interference pattern. The resulting time-dependent modulation of the index of refraction creates a diffraction grating that Bragg-diffracts a variably delayed probe pulse. In this case, z is parallel to the bilayer planes.

the sample through alternate squeezing of two polyethylene wash bottles connected by Teflon tubing through two holes drilled into one of the optical flats (the top one of the sandwich setup). The process was monitored by placing the sample on the stage of a polarizing microscope, in which the aligned regions appear black between crossed polarizers. Once the sample was aligned, the tubes were cut off, leaving $\sim$2 cm of Teflon tubing in each hole. A 50 mM HEPES buffer was then allowed to come into contact with the sample through the holes, and the ends of the tubings were sealed with parafilm. The sample was allowed to rest while the HEPES buffer diffused into the bilayers. This hydration process was monitored by using the LIPS experiment [both the frequency and attenuation of the launched acoustic wave are sensitive to percent hydration (T. A. Guion et al., unpublished results)]. Hydration was assumed to be complete when no change in the frequency and attentuation of the signal was detected in a 0.5-h time period. This usually required 2–3 h.

Cholesterol content in the samples was assayed by a $FeCl_3$ colorimetric assay (Zlattis et al., 1953).

Methods

Briefly, the typical experiment proceeds as follows (see Figure 1). The aligned lipid multibilayers are exposed to two crossed, picosecond excitation pulses having the same wavelength and polarization. Constructive and destructive interference in the crossing volume produces a sinusoidally varying pattern of intensity peaks and nulls, which launches an acoustic standing wave. The acoustic wavelength and orientation match the interference-pattern geometry (Fayer, 1982, 1984). The periodic density (and thus the refractive index) variations associated with the acoustic wave propagation act as a diffraction grating for a variably delayed probe pulse incident at the Bragg angle. The changes in diffracted probe intensity as a function of delay time following the grating excitation are used to calculate the velocity and attenuation of the induced ultrasonic wave (Eyring & Fayer, 1984).

Figure 2 is a schematic representation of the laser setup used in these experiments. The laser is a continuously pumped Nd:YAG oscillator that is acoustooptically mode-locked and Q-switched to produce 1.06-μm pulses at 250 Hz (Fayer,
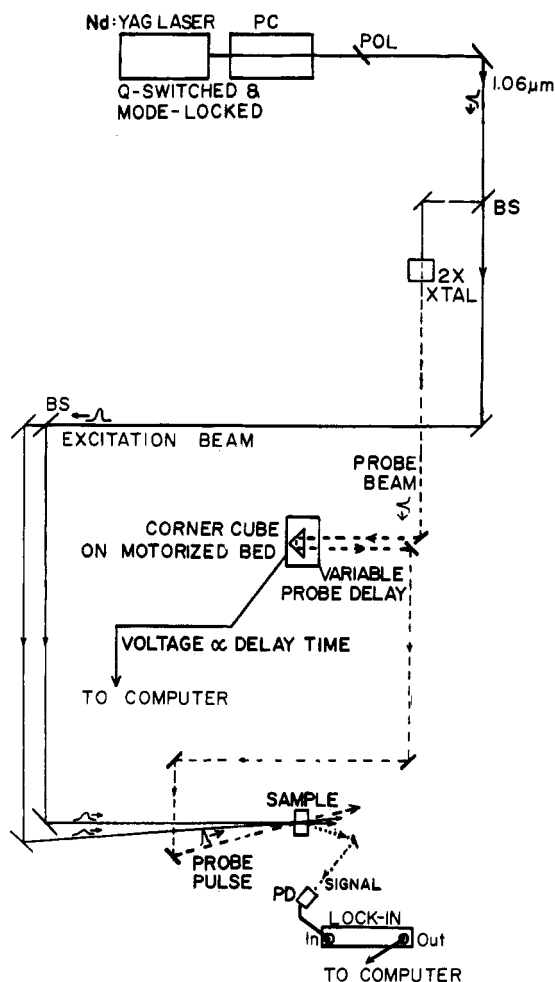
FIGURE 2: LIPS experimental setup. A single 1.06-μm pulse is selected from the YAG mode-locked pulse train. Approximately 80% of the pulse is split into two excitation pulses and recombined at the sample to generate the counterpropagating waves and transient grating. The rest of the single pulse is frequency-doubled to 532 nm and used to probe the grating after a variable delay. The Bragg-diffracted part of the probe pulse is the transient grating signal. PC $\equiv$ Pockel cell; PD $\equiv$ photodiode; BS $\equiv$ beam splitter.

1982). The output is a train of some 40 mode-locked pulses of width 100 ps separated by 12 ns. A 90-μJ pulse is selected from the center of the train by a Pockels cell. Twenty percent of the IR energy is split off and frequency doubled by the CD*A crystal to give a 5-μJ probe pulse at 532 nm. The remaining pulse is beam-split and crossed at an angle θ to produce the interference pattern with a fringe spacing of

$$\Lambda = \lambda/[2 \sin (\theta/2)] \qquad (1)$$

where λ is the IR excitation wavelength (1.06 μm). Λ was kept at 2.50 μm.

The 532-nm probe pulse was delayed by an optical delay line entering the sample 0–20 ns after the excitation pulse. Spot sizes of the IR excitation pulses and the 532-nm probe pulse were 120 and 70 μm, respectively. The diffracted probe was directed into a large-area photodiode, and the signal was amplified by a lock-in amplifier. The lock-in output was digitized and stored with an IBM computer.

THEORY

Laser-Induced Phonons. The LIPS technique involves crossing two excitation laser pulses to optically generate longitudinal (compressional) acoustic waves with a well-defined wave vector and monitoring the resulting density grating with a third probe pulse. This means that both the wavelength and

the propagation direction of the acoustic wave are known. By varying the acoustic wave propagation direction with respect to the bilayer normal, the anisotropic properties of the multilayer are examined. By varying the acoustic wavelength, a range of physical properties can be probed (Nelson et al., 1982).

There are two mechanisms of acoustic wave generation. (1) One is thermal absorption. The sample experiences a weak absorption due to the forbidden $v = 0 \rightarrow v = 3$ C–H stretch transition where the two IR pulses constructively interfere. A rapid relaxation translates this absorption to heat. Thus, on a 100-ps time scale, a sinusoidal temperature variation is set up in the sample. The expansion of the heated areas produces two effects: First, the expansion launches counterpropagation acoustic waves having the grating wave vector. Second, the expansion itself becomes a nonpropagating density grating, less dense in the heated areas and more dense in the unheated areas. This density grating decays by thermal diffusion (microsecond time scale).

Previous estimates (Eyring & Fayer, 1985) show temperature increase in the intensity peaks to be $\sim 10^{-3}$ K per shot. Thus, the generation of the acoustic waves is an extremely mild perturbation of the system.

(2) The other is stimulated Brillouin scattering (SBS). The same crossed IR excitation pulses generate a second set of counterpropagating acoustic waves because of coupling of the electromagnetic field of the laser pulses with the sample through the photoelastic constant. This process, also known as electrostriction, generates longitudinal acoustic waves having the wave vector of the IR interference grating (Nelson, 1982). These acoustic waves differ from the thermally generated acoustic waves only in phase and amplitude.

Thus, density variation produced by the standing longitudinal acoustic waves generated by thermal absorption and SBS add to the nonpropagating thermal density grating. Since in our experiments the system is monitored over 20 ns, the thermal density grating appears to be static. The acoustic waves, on the other hand, propagate and decay on a nanosecond time scale.

These density variations are monitored by a third pulse that is brought into the sample at the Bragg angle to the density grating. The intensity of the Bragg diffracted probe pulse is related to the magnitude of the density variations by (Nelson et al., 1982)

$$I(t) \propto \{A[1 - \cos \omega t \exp(-\alpha Vt)] - B \sin \omega t \exp(-\alpha Vt)\}^2 \qquad (2)$$

where A and B are constants indicating relative amplitudes of the thermal absorption and SBS mechanisms, respectively, and ω is the circular frequency of the traveling acoustic waves having velocity V (cm/s) and attenuation α [neper (Np)/cm]. The damped cosine term corresponds to the thermally generated acoustic wave, and the damped sine term corresponds to the SBS generated wave. Two aspects of this function need to be illuminated. First, since $1 - \cos \omega t = 2 \cos (\omega/2)t$, the thermal absorption term appears to have half the frequency of the SBS term. Second, at long time $t \gg (\alpha V)^{-1}$, $I(t) \propto A^2$; i.e., the probe diffracts only from the static thermal density grating. Figure 3 shows typical data that illustrate the various aspects of eq 2. Figure 3A is for a sample of DPPC with 0 mol % cholesterol at 73 °C, while Figure 3B is for DPPC with 30 mol % cholesterol at the same temperature. In Figure 3B the acoustic damping is considerably faster than in Figure 3A, as evidenced by the more rapid decrease in the size of the oscillations. Notice that between the large peaks at the beginning of the trace are small peaks. The smaller peaks are
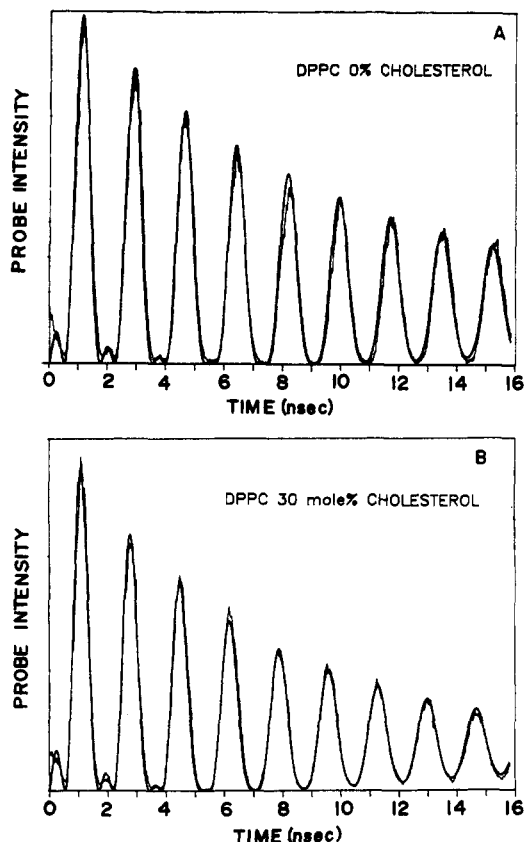
FIGURE 3: Diffracted probe intensity (ragged lines) as a function of probe delay time (nanoseconds) for (A) aligned, fully hydrated DPPC multibilayers and (B) aligned, fully hydrated multibilayers of DPPC with 30 mol % cholesterol. Both scans were taken at 73 °C. Also shown are the least-squares fits to the data (smooth lines).

generated by the SBS mechanism while the large peaks are generated primarily by the heating mechanism with a small contribution from SBS.

The diffraction intensity is recorded, and the four parameters A, B, ω, and αV are obtained by least-squares fitting the LIPS signal to eq 2. Typical plots of fits are shown in Figure 3 by the smooth lines. Although these are four-parameter fits, the parameters are essentially independent, and reproducible fits are obtained, independent of the initial guesses. Since the wavelength of the acoustic waves is given by eq 1, the velocity V and attenuation α are retrieved from ω and αV by using the relationships $\omega = 2\pi f$ and $V = \lambda f$.

Determination of Elastic Stiffness and Viscosity. The two physical constants obtained by the LIPS experiment are acoustic velocity V and attenuation α. The velocity is related to the elastic stiffness constants C_{ij} of the system, while the attenuation reflects relaxation processes that tend to absorb the acoustic energy. Following LePesant et al. (1978), we note that the lipid–water multilayer system is characterized by three elastic constants, denoted by C_{11}, C_{33}, and C_{13}, and can support two acoustic waves with speeds V_1 (transverse) and V_3 (longitudinal). In the work described here the wave vector is in the plane of the bilayer, so that

$$V_1{}^2 = 0 \qquad (3)$$

and

$$V_3{}^2 = \rho^{-1}C_{11} \qquad (4)$$

where ρ is the macroscopic density. V_3 will be designated V, the velocity measured in the experiment. The elastic constant C_{11} is a measure of the area compressibility of the lipid in the bilayer plane at constant layer spacing d:

$$C_{11} = -A(\partial P/\partial A)_d = \rho(\partial P/\partial \rho)_d \qquad (5)$$

where A is the area per molecule and P is the lateral pressure that tends to change A. It is implicit that the derivatives are taken at constant entropy and water concentration.

Acoustic damping has several sources and is written in general as $\alpha = \alpha_\eta + \alpha_i + \alpha_c$, where α_η is the classical viscoelastic damping, α_i is damping due to a coupling with lipid internal degrees of freedom, and α_c is damping due to coupling of the acoustic field with critical fluctuations seen at phase transitions. α_i and α_c are strongly frequency-dependent processes with characteristic relaxation times τ_i. Their contribution to damping is found under the summation in eq 6. α_η accounts for B^∞, which is frequency-independent. The damping α is seen to depend on the square of the frequency and on the relaxation times τ_i according to

$$\alpha/f^2 = B^\infty + \sum_i A_i{}^0\tau_i(1 - \omega^2\tau_i{}^2)^{-1} \qquad (6)$$

where B^∞ describes the limiting viscosity at high frequency. Gamble and Schimmel (1978) fit their ultrasonic absorption data on DPPC vesicles near the phase transition temperature with a single relaxation time of 10 ns (16 MHz) and saw no relaxation processes above 150 MHz. Since our study involved 600-MHz waves, eq 6 reduces to

$$\alpha/f^2 = B^\infty \qquad (7)$$

Thus we expect to see no critical damping in the region of the phase transition or frequency-dependent damping due to rotational isomerization of the lipid chains.

The damping constant, B^∞, is related to the elements of the viscosity tensor. Just as with the acoustic velocity, the symmetry of the multibilayer array requires that the attenuation be anisotropic; i.e., its magnitude depends on the acoustic wave vector (Martin et al., 1972). For the case of longitudinal waves propagating in the plane of the bilayer, the expression for α/f^2 simplifies to (Candau & Letcher, 1978)

$$\alpha/f^2 = \frac{2\pi^2}{\rho V^3}(\eta_2 + \eta_4) = \frac{2\pi^2}{\rho V^3}\eta_{11} \qquad (8)$$

where η_2 and η_4 are two of the five viscosities required to describe a compressible smectic system, in the notation of Martin et al. (1972), and η_{11} is equivalent to their sum (Forster et al., 1971). η_4 is the in-plane shear viscosity, where η_2 has contributions from the volume viscosity. The membrane viscosities obtained from ultrasonic attenuation measurements are not directly comparable to the microviscosities deduced from rotational and translation diffusion studies (Shimshick & McConnell, 1973; Shinitzky & Barenholz, 1978) since the latter are more or less related to the shear viscosity. However, a comparison can be made by using eq 8 and noting that in most liquids $\eta_4 \cong \eta_2$ in the high-frequency range (Candau & Letcher, (1978). For example, in the nematic phase of the liquid crystal MBBA [N-(-p-methoxybenzylidene)-p-butylaniline], the shear and volume viscosities have been independently measured (Candau & Letcher, 1978). It is found that $\eta_2 = 0.41$ P and $\eta_4 = 0.43$ P. Therefore, for comparison purposes it is reasonable to take the shear viscosity to be ($\eta_2 + \eta_4$)/2 = η_{11}/2.

Densities in eq 8 and 5 were obtained from Gershfeld (1978). The error introduced into C_{11} and η_{11} by uncertainty in the density is always less than half the experimental error. The experimental error in ω values was generally very small (<2%) and insensitive to the signal to noise ratio (S/N) in the LIPS scans. However, the αV values had a larger experimental error (<15%) and were found to be sensitive to the quality of
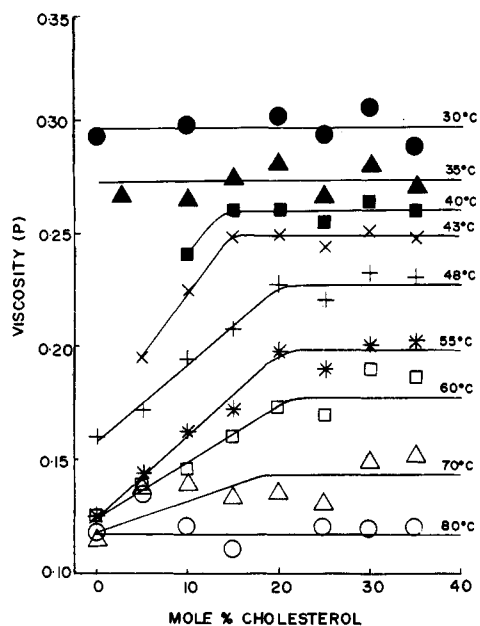
FIGURE 4: Effect of increasing cholesterol content in multibilayers on the anisotropic bulk viscosity (η) at different temperatures: O represents data points taken at 80 °C, ▲ at 70 °C, □ at 60 °C, * at 55 °C, + at 47.5 °C, × at 42.5 °C, ■ at 40 °C, ▲ at 35 °C, and ● at 30 °C. The lines joining the points are intended only as aids in examining the data.

the scan. To improve the S/N ratio, multiple scans were averaged at each temperature point examined, and the fit of the averaged scan was reported. The error at each temperature point was estimated from the fitted values obtained from the scans before averaging. In general, larger errors were noticed in the vicinity of the phase transition temperature of the lipid.

RESULTS

Cholesterol Effects on Viscosity (η_{11}). The effect of cholesterol content on the viscosity (eq 8) of the DPPC bilayers at various temperatures is shown in Figure 4. In the liquid-crystalline phase, the viscosity increases with increasing cholesterol, up to $\sim$22 mol % cholesterol, after which increasing cholesterol content has no further effect on the viscosity. The initial increase in viscosity agrees with the established behavior of the changes detected in "microviscosities" of bilayers as measured by other techniques (Jain, 1975) under similar conditions. Cholesterol incorporation into a lipid bilayer in the gel phase is reported to decrease the "microviscosity" (Jain, 1975). We detect no measurable change in the viscosity in the gel phase (Figure 4). This result will be discussed later in this report.

Another notable trend in Figure 4 is that the changes in η_{11} due to cholesterol incorporation in the multibilayers are at a maximum in the vicinity of T_c, decreasing as the temperature is increased above T_c, showing no change by 80 °C, and decreasing when the temperature is decreased below T_c, showing no change by 35 °C. This kind of behavior agrees with the concept that the lipid bilayer is most susceptible to cholesterol perturbations in the vicinity of the phase transition temperature since cholesterol is thought to disrupt the cooperativity between the hydrocarbon chains (Presti et al., 1982).

Cholesterol Effect on Elastic Stiffness (C_{11}). Figure 5 shows the changes in the elasticity of DPPC bilayers as cholesterol content is increased at various temperatures.

In the liquid-crystalline phase, incorporation of cholesterol in the bilayer up to 10 mol % has no measurable effect on the C_{11}. An increase in C_{11} is noticed as cholesterol concentrations are increased from 15 to $\sim$20 mol %. Further increasing the
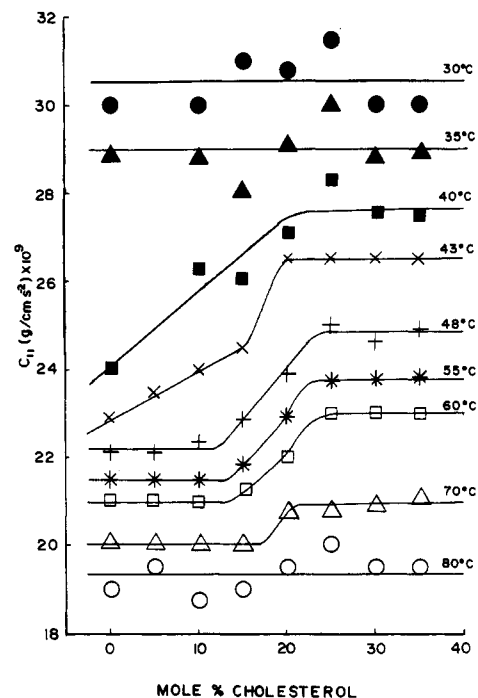

FIGURE 5: Effect of increasing cholesterol content in DPPC multibilayers on the anisotropic bulk modulus C_{11} at different temperatures. Notations are the same as in Figure 4. The lines joining the points are intended only as aids in examining the data.

cholesterol concentration has little or no further effect on the measured C_{11}. In the vicinity of the phase transition temperature (40 and 43 °C) the C_{11} measurements, like the η_{11} measurements, are more sensitive to cholesterol presence, where a linear increase of C_{11} values with increasing cholesterol concentrations is noticed until $\sim$20 mol % cholesterol. Below the phase transition temperature, the C_{11} parameter responds in an analogous manner to the viscosity, showing no measurable changes in the presence of cholesterol.

Cholesterol Effects on Phospholipid Phase Transition. The presence of cholesterol has been reported to broaden the first-order phase transition of lipid bilayers (Jain, 1975). This phenomenon is seen in both the viscosity (Figure 6) and the elastic stiffness (Figure 7) measurements. The phase transition break at 41.5 °C for DPPC multibilayers in the absence of cholesterol is particularly apparent in Figure 6, where a nonlinear behavior of viscosity vs. temperature is noticed. As cholesterol is introduced into the multibilayers, the break becomes less obvious, and by 20 mol % cholesterol, its presence is questionable in view of the error in our measurements (Figure 6). In bilayers, where the cholesterol content is higher than 20 mol %, the η_{11} appears to increase linearly with decreasing temperature.

A similar though less obvious trend can also be followed with the C_{11} data (Figure 7). In the absence of cholesterol, a larger increase in C_{11} ($\sim$8 × 10⁹ g cm⁻¹ s⁻²) is noticed as the lipid goes through its phase transition. As cholesterol content is increased, that increase in C_{11} decreases until $\sim$20 mol % cholesterol where it levels off at $\sim$4 × 10⁹ g cm⁻¹ s⁻². However, unlike the viscosity measurements, a linear dependence is not reached in the cholesterol concentration range examined (0–35 mol %).

DISCUSSION

There exist in the literature only a few papers where measurements of vesicle/bilayer bulk viscoelastic properties are reported. Mitaku et al. (1978) reported the bulk modulus K of DPPC multilamellar vesicles at various temperatures with
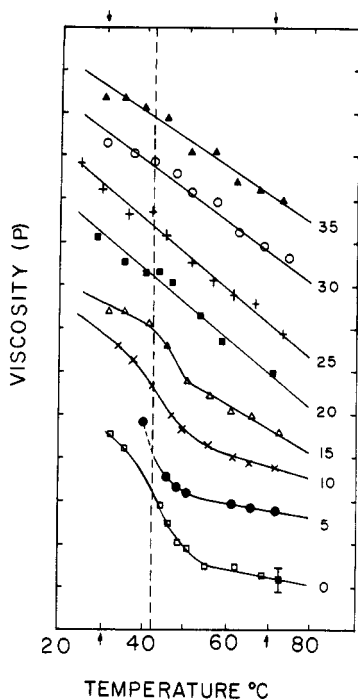
FIGURE 6: Temperature dependence of the in-plane viscosity of fully hydrated, aligned DPPC multibilayers with different cholesterol concentrations. The various plots are displaced along the y axis and stacked one on top of the other. The numbers on the side represent the cholesterol concentration in mole percent. The viscosity values shown are calculated from the fit of the average of two or three LIPS scans. Error was estimated as described in the text. Typical error obtained is shown in the 0 mol % cholesterol scan at ~70 °C. The lines drawn between the points are only to guide the eye. The dotted line represents the T_c of pure, fully hydrated DPPC multibilayers. The range of viscosity change from 30 to 70 °C (temperatures marked by arrows) for the sample is as follows: 0 mol %, 0.29–0.11 P; 5 mol %, 0.29–0.14 P; 10 mol %, 0.29–0.14 P; 15 mol %, 0.29–0.13 P; 20 mol %, 0.3–0.135 P; 25 mol %, 0.29–0.13 P; 30 mol %, 0.3–0.17 P; 35 mol %, 0.29–0.16 P. This information enables the estimation of the viscosity at any point on the plot; e.g., the viscosity of a DPPC sample with 20 mol % cholesterol at 55 °C is 0.2 P.

a differential ultrasonic velocimeter. The value of K is calculated as $K = \rho V^2$ as is C_{11} in our work. Since the differential velocimeter generates acoustic waves at all orientations to the bilayer normal, the bulk modulus K differs from the elastic constant C_{11} measured in this work in that K is an average of all the elastic constants C_{ij}. Their data indicate an anomalous dip of K at the phase transition temperature, which is not seen in our experiments. In a similar set of experiments performed by Maynard (1985), a peak in acoustic absorption was seen at the phase transition of DPPC/DPPG (dipalmitoylphosphatidylglycerol) multilamellar vesicles. Both experiments probed the systems with 3-MHz longitudinal ultrasonic waves. As pointed out under Theory of this paper, an "anomalous" peak is not expected in our C_{11} or acoustic absorption measurements since the vastly higher acoustic frequencies used in our experiments (600 MHz) are not expected to couple with any critical phenomena.

Sakanishi et al. (1979), using a setup similar to that of Mitaku et al. (1978), have estimated the bulk modulus K of sonicated DPPC vesicles with varying cholesterol concentrations. Table I compares their K values to the C_{11} values obtained in this work. Table I also includes values of C_{11} obtained from Brillouin scattering experiments performed by LePesant et al. (1978) on aligned DPPC multibilayers. There is a remarkable agreement between all three techniques at temperatures where the lipid bilayer exists in the liquid-crystalline phase. However, a difference is observed in the gel
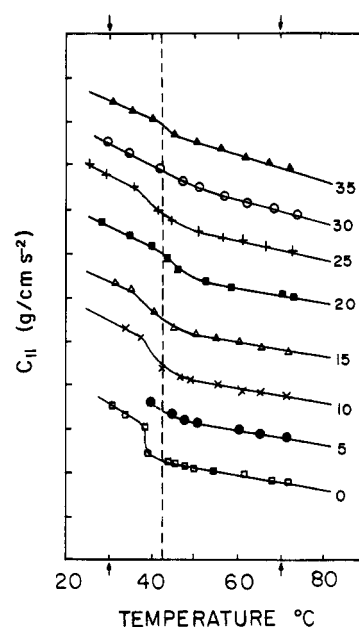

FIGURE 7: Temperature dependence of C_{11} of fully hydrated DPPC multibilayers with different cholesterol contents. The various plots are displaced along the y axis and stacked one on top of the other. The notations are the same as in Figure 6. The error in these measurements was generally within the limits of the points drawn. The range of C_{11} change from 30 to 70 °C for the sample with varying cholesterol concentrations is as follows: 0 mol %, (30–20) $\times 10^9$ g cm^{-1} s^{-2}; 5 mol %, 30–20; 10 mol %, 30–20; 15 mol %, 30–20; 20 mol %, 31–21; 25 mol %, 31–21; 30 mol %, 30–21; 35 mol %, 30–21. This information enables the estimation of C_{11} at any point on the plot.

Table I: Elastic Stiffness Measurements by Different Techniques

elastic stiffness ($\times 10$ dyn^2/cm)	liquid-crystalline phase (50 °C)		gel phase (30 °C)	
	DPPC	DPPC + cholesterol	DPPC	DPPC + cholesterol
K^a	2.20	2.50^d	2.77	2.68^d
$C_{11}{}^b$	2.20	2.50^e	3.30	3.10^e
$C_{11}{}^c$	2.20	2.50^f	3.05	2.90^f

[a]Sakanishi et al., 1979. [b]LePesant et al., 1978. [c]This work. [d]Forty-nine mole percent cholesterol in bilayers. [e]Thirty-three mole percent cholesterol in bilayers. [f]Thirty-five mole percent cholesterol in bilayers.

phase. The difference between the K values reported by Sakanishi et al. (1979) and the C_{11} values reported here and by LePesant et al. (1978) can be explained by the difference in the definition of K, which measures the elastic response to acoustic waves traveling at all orientations to the bilayer, and C_{11}, which measures the elastic response to waves traveling only in the bilayer plane. Acoustic waves having a vector component normal to the bilayer may not experience the stiffening effect of the phase transition to the same extent as acoustic waves with in-plane wave vectors. Thus K would be expected to be lower than C_{11} for the same system. The difference between our C_{11} values and those of LePesant et al. could be caused by the sensitivity of both techniques to the optical quality of the sample. The poor optical quality of the gel phase of DPPC multibilayers greatly increases the scattered light, resulting in a decreased signal to noise ratio. This problem is more severe for the Brillouin scattering than for the LIPS technique.

The term microviscosity has been used to describe the fluidity of biomembranes. The literature documents a wide range of values for this parameter. For example, fluorescent spectroscopy, with perylene as a probe, obtained a value of

1 P for DPPC dispersions at 45 °C (Cogan et al., 1973), while with pyrene as a probe, it obtained a value of 0.6 P for dimyristoylphosphatidylcholine (DMPC) dispersions at 30 °C (Vanderkooi, 1974). ^{13}C NMR data on DMPC sonicated dispersions at 52 °C estimate a microviscosity near the center of the bilayer of 2.4 P (Lee, 1975). It is important to remember that all these measurements mainly reflect the orientational constraints of the probe in the bilayer and they do not directly reflect the anisotropic bulk viscosity in the bilayer plane. The experiments presented here are the first to directly measure the bulk viscosity in the plane of the lipid bilayer. These measurements of the bulk η_{11} on DPPC multibilayers are a factor of 10–15 smaller than the previously reported microviscosities. (Typical values from our experiments are 0.1–0.15 P.) These differences emphasize that the microviscosity and the bulk viscosities of lipids are two very different properties and that one should not project from one to the other without extreme caution.

The generally accepted view of phospholipid/cholesterol interaction is that cholesterol has a "fluidizing" effect on the phospholipid bilayer below T_c and a "gelling" effect above T_c, such that at ~20 mol % cholesterol the cooperativity of the lipid-chain melting at the phase transition temperature has been removed and a state of intermediate fluidity is maintained that is relatively insensitive to temperature changes (Jain, (1975). This phenomenon has been called the "dual effect" of cholesterol and has been observed within 5 °C above and below the T_c of the phospholipid.

Our η_{11} and C_{11} measurements support the "gelling" effect seen with the addition of cholesterol to DPPC multibilayers above T_c. However, in the gel state, addition of cholesterol showed no decrease in the measured C_{11} or η_{11}. Furthermore, though cholesterol did abolish the cooperativity of the hydrocarbon-chain melting at ~20 mol % (as detected by the disappearance of the sharp break in viscosity around T_c, Figures 6 and 7), the resulting state was still temperature sensitive, showing a decrease in C_{11} and η_{11} with increasing temperature. This strongly suggests that the "dual effect" of cholesterol as measured by local fluctuations is not a macroscopic phenomenon.

The various special effects measured at 20 mol % cholesterol by different physical techniques (Jain, 1975) have recently been incorporated into a molecular model proposed by Presti et al. (1982). This model proposes a molecular separation below 20 mol % cholesterol, where cholesterol–phospholipid complexes (1:2) coexist with free phospholipid domains. This separation is hypothesized to cease at 20 mol % cholesterol, at which concentration the free phospholipid domains are hypothesized to disappear. It is important to note that while this is a microscopic model, we detect changes in bulk properties of the multibilayers, i.e., the viscosity η_{11} and elastic stiffness C_{11}, in the vicinity of 20 mol % cholesterol (Figures 4 and 5). This suggests that the model describes changes in the macroscopic as well as microscopic properties of these systems.

A recent article by Knoll et al. (1985) reports small-angle neutron scattering (SANS) and freeze–fracture electron microscopy work on DMPC–cholesterol mixed vesicles. Their work does not indicate phase separation below 20 mol % cholesterol at temperatures above the T_c of the lipid. It is therefore in variance with the conclusions based on previous spectroscopic techniques. The authors argue that the molecular motions measured by these techniques depend on the local packing density of the lipid molecules and that nonideal behavior of the molar areas (or volumes) of a mixture may lead to breaks in the probe partitioning [e.g., the ESR probe 2,2,6,6-tetramethylpiperidinyl-1-oxy (TEMPO)] or molecular mobilities. It is suggested that these could be erroneously interpreted in terms of phase boundaries. The LIPS technique used in this work measures bulk properties and is not sensitive to such local inhomogeneities, and yet we see a change in the trends of our data above T_c, at ~20 mol % cholesterol (Figures 4 and 5). Although the observed trends cannot be proven to be indicative of phase separations, they lend additional credibility to the results obtained with spectroscopic techniques, demonstrating that the anomalies reported by these techniques above T_c, at 20 mol % cholesterol, are not due to inhomogeneous probe distributions but reflect actual properties of the bilayers under investigation.

Hui and He (1983), using X-ray and electron diffraction, have monitored the increase in the width of the wide-angle diffraction signal as the cholesterol concentration is increased in DMPC. By associating the diffraction peak with the coherence length of lipid packing, they conclude that addition of cholesterol decreases the coherence length of lipid packing up to ~20 mol % cholesterol, where a limit in cooperation between DMPC molecules is reached. Hui and He argue that their results are compatible with the Presti model and thus may be interpreted as a quantification of the model. What is remarkable is the high degree of correlation between the coherence length of the DMPC molecules measured by Hui and He and our measurement of the in-plane viscosity of DPPC. This correlation suggests a molecular interpretation for the behavior of the in-plane bulk viscosity.

The LIPS experiment described here allows the examination of the anisotropic bulk properties of lipid multibilayers. We have reported quantitative values of the elastic stiffness and viscosity of these model membranes as a function of cholesterol concentration and temperature. These are important parameters in model membrane studies, which previously have been unobtainable or extrapolated from molecular models. This work emphasizes the difference between the anisotropic bulk and microscopic properties of lipid multibilayers. The value obtained for the viscosity of fully hydrated DPPC multibilayers was an order of magnitude smaller than reported microviscosities. Furthermore, the trends in C_{11} and η_{11} measurements did not always follow those reported in local "fluidity" measurements or order parameters. It is not within the scope of this work to propose a model that accounts for the difference between the microscopic observables and the bulk properties of DPPC–cholesterol multibilayers. However, the results presented here provide a different perspective from which to examine the viscoelastic properties of these model systems.

REFERENCES

Asher, S. A., & Pershan, P. S. (1979) *Biophys. J. 27*, 393.
Blank, M. J. (1962) *J. Phys. Chem. 66*, 1911.
Blank, M., & Britten, J. S. (1965) *J. Colloid Sci. 20*, 789.
Candau, S., & Letcher, S. V. (1978) *Adv. Liq. Cryst. 3*, 167.
Cogan, U., Shinitzky, M., Weber, G., & Nishida, T. (1973) *Biochemistry 12*, 521.

Copeland, B. R., & McConnell, H. M. (1980) *Biochim. Biophys. Acta 599*, 95.

Cortijo, M., & Chapman, D. (1981) *FEBS Lett. 131*, 245.

Crilly, J. F., & Earnshaw, J. C. (1983) *Biophys. J. 41*, 211.

Cullis, P. R. (1976) *FEBS Lett. 70*, 223.

Demel, R. A., & De Kruijff, B. (1976) *Biochim. Biophys. Acta 457*, 109.

Estep, T. N., Mountcastle, D. B., Bittonen, R. L., & Thompson, T. E. (1978) *Biochemistry 17*, 1984.

Eyring, G., & Fayer, M. D. (1984) *J. Chem. Phys. 81*, 4314.

Eyring, G., & Fayer, M. D. (1985) *Biophys. J. 47*, 37.

Fayer, M. D. (1982) *Annu. Rev. Phys. Chem. 33*, 63.

Fayer, M. D. (1984) *IEEE J. Quantum Electron.* (in press).

Forster, D., Lubensky, T. C., Martin, P. C., Swoft, J., & Pershan, P. S. (1971) *Phys. Rev. Lett. 26*, 1016.

Gamble, R. C., & Schimmel, P. R. (1978) *Proc. Natl. Acad. Sci. U.S.A. 75*, 3011.

Gershfeld, N. L. (1978) *Biophys. J. 22*, 469.

Hui, S. W., & He, N. B. (1983) *Biochemistry 22*, 1159.

Jain, M. K. (1975) *Curr. Top. Membr. Transp. 6*, 1.

Knoll, W., Schmidt, G., Ibel, K., & Sackmann, E. (1985) *Biochemistry 24*, 5240.

Lee, A. G. (1975) *Prog. Biophys. Mol. Biol. 29*, 3.

Lentz, B. R., Barrow, D. A., & Hoechli, M. (1980) *Biochemistry 19*, 1943.

LePesant, J. P., Powers, L., & Pershan, P. S. (1978) *Proc. Natl. Acad. Sci. U.S.A. 75*, 1792.

Mabrey, S., Mateo, P. L., & Sturtevant, J. M. (1978) *Biochemistry 17*, 2464.

Martin, P. C., Parodi, O., & Pershan, P. S. (1972) *Phys. Rev. A 6*, 2401.

Maynard, V. (1985) *Chem. Phys. Lett. 37*, 1.

Mitaku, S., Ikegami, A., & Sakanishi, A. (1978) *Biophys. Chem. 8*, 295.

Nelson, K. A. (1982) *J. Appl. Phys. 53*, 6060.

Nelson, K. A., Casalegno, R., Miller, R. J. D., & Fayer, M. D. (1982) *J. Chem. Phys. 77*, 1144.

Papahadjopoulos, D., Jacobson, K., Nir, S., & Isac, T. (1973) *Biochim. Biophys. Acta 311*, 330.

Phillips, M. C. (1972) *Prog. Surf. Membr. Sci. 5*, 139.

Powers, L., & Clark, N. A. (1975) *Proc. Natl. Acad. Sci. U.S.A. 72*, 840.

Presti, F., Pace, R. J., & Chan, S. I. (1982) *Biochemistry 21*, 3831.

Recktenwald, D. J., & McConnell, H. M. (1981) *Biochemistry 20*, 4505.

Sakanishi, A., Mitaku, S., & Ikegami, A. (1979) *Biochemistry 18*, 2636.

Schreier, S., Polnasek, C. F., & Smith, I. C. P. (1978) *Biochim. Biophys. Acta 515*, 375.

Shimshick, E. J., & McConnell, H. M. (1973) *Biochem. Biophys. Res. Commun. 53*, 446.

Shinitzky, M., & Barenholz, Y. (1978) *Biochim. Biophys. Acta 515*, 367.

Shinitzky, M., Skornick, E., Gorelik, E., & Sindelar, W. (1983a) *Prog. Clin. Biol. Res. 132*, 425.

Shinitzky, M., Lyte, M., Heron, D. S., & Samuel, D. (1983b) *Mod. Aging Res. 3B*, 175.

Tilcock, C. P. S., Bally, M. B., Farren, S. B., & Cullis, P. R. (1982) *Biochemistry 21*, 4596.

Vanderkooi, J. M. (1974) *Biochemistry 13*, 4000.

Zlattis, A., Zak, B., & Boyle, A. J. (1953) *J. Lab. Clin. Med. 41*, 486.